ACS APPLIED MATERIALS & INTERFACES

Research Article

www.acsami.org

Growth of Nanobipyramid by Using Large Sized Au Decahedra as Seeds

Guangju Zhou,[†,‡] Yun Yang,*[,†] Shuhua Han,[†] Wei Chen,[†] Yunzhi Fu,[‡] Chao Zou,[†] Lijie Zhang,[†] and Shaoming Huang*[,†]

[†]Nanomaterials and Chemistry Key Laboratory, Wenzhou University, Wenzhou, Zhejiang 325027, P. R. China

[‡]Hainan University, College of Materials and Chemical Engineering Hainan Haikou 570228, P. R. China

Supporting Information

ABSTRACT: Au nanobipyramids (NBPs) are important nanostructures which attract much attention due to their unique structure, optical, and catalytic properties. The controlled synthesis of Au NBPs and corresponding mechanistic study are highly desirable for both fundamental research and practical applications. Herein, we demonstrate a strategy that large sized Au decahedra with well-defined shape act as seeds for growing NBPs. Furthermore, through using different sized decahedra seeds with edge from 25 to 49 nm, various sized NBPs can be easily prepared (longitudinal length from 110 to 210 nm; transverse length from 36 to 70 nm). Our study provides hard evidence for the growth of NBPs that they surely stem from the overgrowth on penta-twinned decahedra. Because these used large size seeds have well-defined shape and structure, the growth of the NBPs can be easily determined. Results show that the formation of NBPs is primarily determined by the molar ratio of Au^{3+} and Au seeds (MRAA). MRAA less than 4 only causes size enhancement and no significant shape change. In cases of MRAA higher than 4 and lower than 8, quasi-nanorods are produced. When MRAA range from 8 to 10, NBPs form and the yield is higher than 90%. The effect of reaction time and temperature also are vital to the growth of NBPs. These prepared NBPs are found to exhibit excellent surface enhanced Raman scattering (SERS) performance because of many present hotspots, edges, steps, and tips on their surfaces.

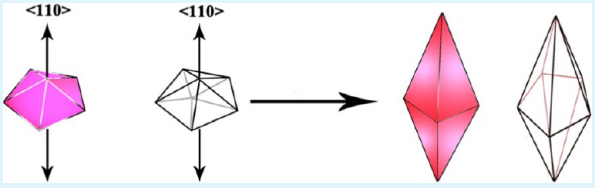

KEYWORDS: *noble, gold, seeded growth, decahedron, nanobipyramid*

1. INTRODUCTION

Noble nanostructures have attracted much attention during the past several decades owing to their promising applications in catalysis, optics, and biosystems.[1−5] As is well-known, their properties and applications are closely related with structures, shapes, sizes, and compositions.[4,6,7] Therefore, numerous efforts have been put into their controlled synthesis and a variety of technologies have been developed successfully.[8−11] Among them, seeded growth is the most popular method.[9,12−18] Generally, seeded growth involves two steps according to reaction sequence, the preparation of small sized nanostructures serving as seeds and the selective growth of other metal atoms on seeds surface. It is a very effective tool for synthesizing various nanostructures including core@shell, alloy, dumbbell-like, island-like, and other heterostructures.[12,19−28] In fact, seeded growth also is an ideal mode for mechanistic study, especially in the case that large sized seeds are used. For the case that small sized seeds are used, clearly understanding growth is a challenging issue for it is difficult to determine the shapes of seeds. To precisely identify the shape of small sized nanoparticles (NPs), high resolution transmission electron microscopy (HRTEM) tomography must be used.[2,30] However, for large sized seeds bounded by well-defined facets, scanning electron microscopy (SEM) and transmission electron microscopy (TEM) allow observing their shapes clearly even at low magnification.[31−36,42] Through comparing the shape difference of products and seeds, it is easy to determine which direction the growth prefers. For example, when {111}-faceted Au octahedra serve as seeds for Ag or Pd deposition and {100}-faceted Au@Ag or Au@Pd nanocubes form, a conclusion that the growth along ⟨111⟩ is favored can be reached.[12,31−33] Song's group synthesized uniform Au nanorods by overgrowing Au on Au decahedra with well-defined shape and the growth preference was along ⟨110⟩ according to product shape.[34] Tsuji's group reported similar results.[35,36]

Au NBPs have interested many scientists working in chemistry, physics, and material science owing to their unique structure and property.[37−42] So far, the most classical synthesis of NBPs involves using Au NPs smaller than 5 nm as seeds. In those small sized seeds, a twinned interface is often observed with HRTEM and hereby they are generally recognized as decahedra.[39] Therefore, Liu and co-workers proposed that the free-defect overgrowth on decahedra produces NBPs. This mechanism is reasonable and successfully explains the structure of NBP. However, other shaped NPs also have twinned feature in practice.[43] Besides, it is not easy to precisely distinguish them

Received: October 1, 2013
Accepted: November 18, 2013
Published: November 18, 2013

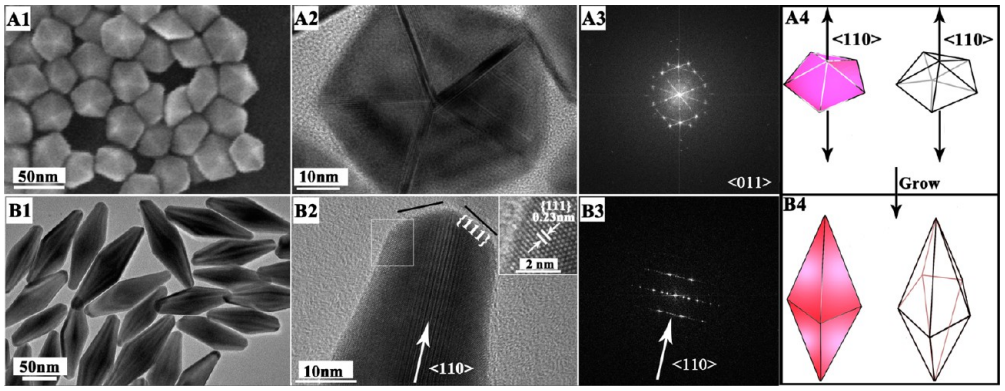

Figure 1. (A1) SEM image of decahedral seeds with 30 nm edge. (A2 and A3) HRTEM image of one decahedron and corresponding FFT pattern. (A4) Sketch of decahedron. (B1) TEM image of NBPs. (B2 and B3) HRTEM image of one NBP and corresponding FFT pattern. (B4) Sketch of NBP. (inset) HRTEM image of area marked by the box. MRAA was 10.

when they are very small and not properly oriented on TEM sample supporter.[39] Other shaped products rather than NBP also form considerably in classical method, indicating that seeds with a twinned interface might have different shapes instead of decahedron. Therefore, the mechanism has uncertainty and needs further evidence to support. There is another issue that the synthesis of NBPs with controlled size and uniform shape is still difficult to achieve so far and most of products always are sphere-like NPs. Such products are very critical to studying the shape- or size-dependent collective properties of materials.[44]

Recently, our group developed a method with which Au decahedra with large size and uniform shape could be synthesized.[45] These large sized decahedra have well-defined shape uniformly and their crystal shapes can be identified easily with high angel annular dark field (HAADF), SEM, and TEM technologies. If above mechanism about the growth of NBP works well,[39] these Au decahedra possibly could act as seeds for growing NBPs. In this study, we demonstrate the feasibility of this strategy and the present study might have significances in two respects. **(1) The syntheses of NBPs with controlled size and uniform shape.** Our method allows controllably synthesizing NBPs with high yield (>90%). Various sized NBPs can be prepared through adjusting decahedral seed sizes. For example, the longitudinal length can be tuned in the regime of 110−210 nm. These NBPs with uniform shape could serve as ideal materials for collective property and application study.[37,38] **(2) Hard evidence for the growth of NBP.** These large sized seeds have well-defined decahedron shape, which allows easily knowing the growth by comparing the shape difference between products and seeds.[35,36] The successful preparation of NBPs with the method reported here provides direct and hard evidence for the growth mechanism of NBP that they surely stem from the overgrowth on penta-twinned decahedra.[39] We investigated the shape-dependent SERS performance of the prepared nanostructures and the result shows that NBPs are better SERS substrate materials than decahedra. Even at very low concentration of probe molecules, Raman signal can be clearly detected.

2. EXPERIMENTAL SECTION

Chemicals. Poly(diallyldimethylammonium chloride) (PDDA, M_w =400 000−500 000, 20 wt % in H_2O), poly(vinylpyrrolidone) (PVP, MW=58000), cetyltrimethylammonium chloride (CTAC), $AgNO_3$, and $HAuCl_4$ were bought from Sigma-Aldrich. Aqueous ammonia and diethylene glycol (DEG) were purchased from Aladdin reagent. All chemicals were used as received, and no purification was performed. Deionized water (18.2 MΩ·cm) was yielded by Milli-Q Academic water purification system (Millipore Corp., Billerica, MA, USA) and used in all experiments.

Preparations of Decahedra with Various Sizes. The preparations of decahedra followed our method reported previously.[45,46] Typically, 5 uL aqueous $HAuCl_4$ (0.48 M) was heated in 125 °C oven to remove water completely and then 10 mL DEG containing 0.25 mL PDDA was added. The solution was stirred vigorously until a yellow homogeneous solution formed. A 3 mL portion of DEG containing 6 mg $AgNO_3$ was then added and the mixture was stirred for another 3 min. The resulting solution was heated in oil bath without disturbance. Through controlling reaction temperature, various sized decahedra could be prepared (224 °C for decahedra with 25 nm edge, 220 °C for decahedra with 33 nm edge, 214 °C for decahedra with 37 nm edge, 200 °C for decahedra with 49 nm edge). After 30 min, the solution was cooled down to room temperature and then 12 mL water was added to dilute the colloid. The resulting colloid solution was used as seeds for the syntheses of NBPs. For TEM sample preparation, 1 mL prepared colloid was mixed with 9 mL water and meanwhile a few drops of concentrated ammonia were introduced to remove AgCl. The products were collected with centrifuge (12000 rpm) and then dispersed into 10 mL water again. The washing was repeated for three times and finally the products were dispersed in 0.5 mL water.

Growth of NBPs. In a standard preparation, 10 uL aqueous ammonia (20% volume ratio) was introduced into a solution (0.5 mL water, 0.5 mL DEG, 1 mL Au seeds (0.000243 mmol), 8 uL PDDA, 0.00136 mmoL $AgNO_3$) and then aqueous $HAuCl_4$ (MRAA is 8 or 10) was added as precursor under vigorous stirring. The resulting mixture was sealed in 10 mL bottle and heated in 90 °C oven for facilitating the growth of NBPs. After 2 h, the heating was stopped and the solution containing NBPs was cooled to room temperature. A similar washing to that of decahedra seeds was used to purify the products.

Surface Enhanced Raman Scattering (SERS) Measurement. Briefly, 100 uL purified colloid containing Au decahedra or NBPs was dropped onto a Si wafer and then heated at 60 °C to remove water completely. The Si wafer supporting nanomaterials was immersed in beaker containing 5 mL ethanol containing 2-naphthalenethiol. A period of 10 h later, the Si wafer was washed using ethanol for 3 times to remove absorbed 2-naphthalenethiol. After the Si wafer was dried at 50 °C for 30 min, it was used as SERS investigation.

Characterization. For sample preparations of TEM and HRTEM, the purified colloid was deposited on carbon-membrane-coated copper grids and dried for 30 min at 80 °C. After the solvent was removed completely, it was observed on 200 KV JEOL 2100F microscope. The HAADF images and energy dispersive spectroscopy (EDS) were obtained with 300KV Tecnai G2 F30 S-Twin microscope with an attached scanning transmission electron microscopy (STEM) EDS system. The UV−vis spectra of colloid nanostructures were recorded

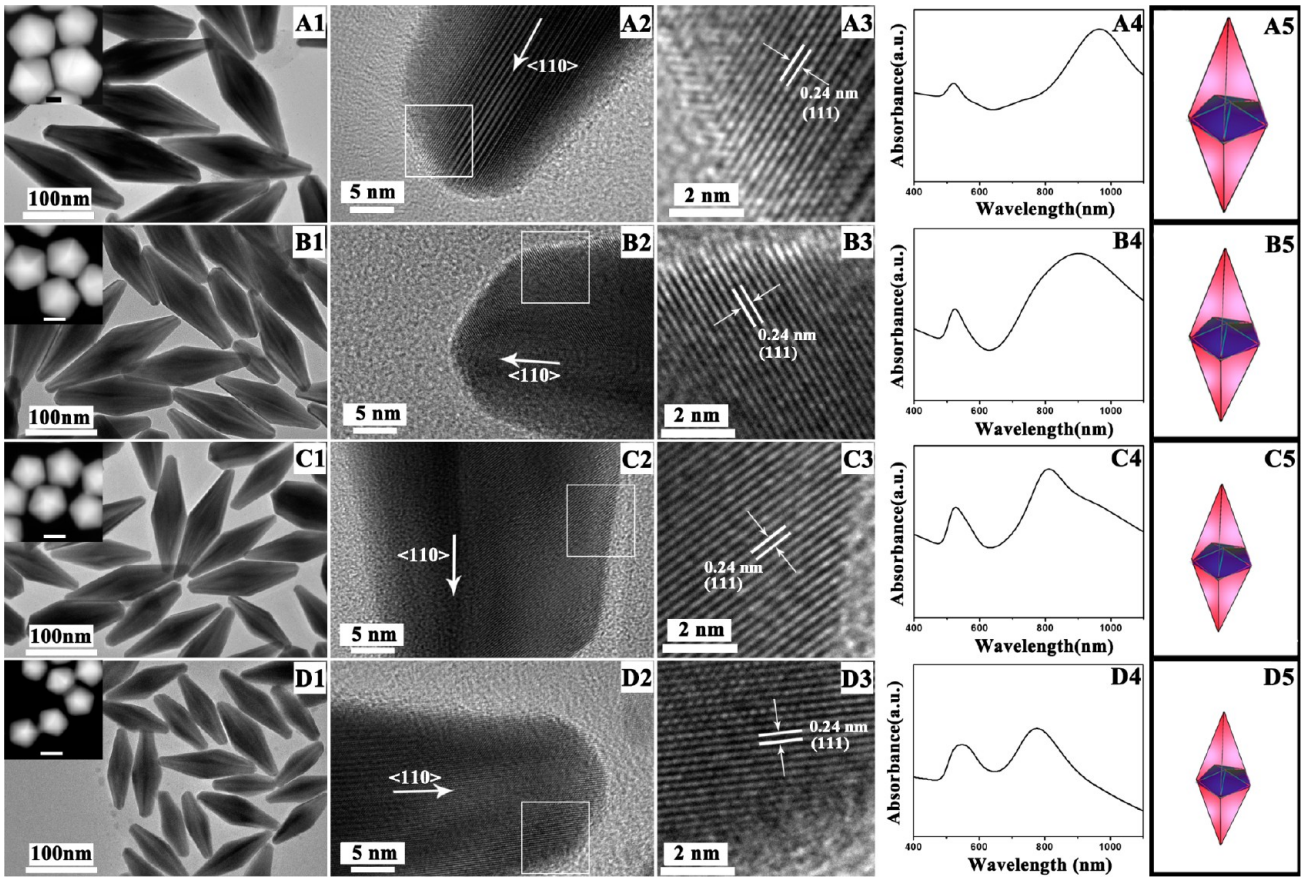

Figure 2. Typical TEM images, HRTEM images, UV−vis spectra, and sketches of Au NBPs prepared using Au decahedra with various sizes as seeds: (A1−A5) 49 nm edge (MRAA was 9); (B1−B5) 37 nm (MRAA was 9); (C1−C5) 33 nm (MRAA was 10); (D1-D5) 25 nm (MRAA was 10). (insets) HAADF images of decahedra seeds and the scale bars are 25 nm. The squares (A2, B2, C2, and D2) mark the area of HRTEM image (A3, B3, C3, and D3).

with a Shimadzu 2450 UV−vis spectrophotometer at room temperature. Raman measurement was taken by RENISHAW rama-scope microraman system at room temperature (633 nm Ar^+ laser line excitation, 5 mW).

3. RESULTS AND DISCUSSION

Overgrowth on Au Decahedra along ⟨110⟩ into NBPs with Controlled Size. The growth solution is a mixture of DEG (reducing agent), water, PDDA (stabilizing agent), $AgNO_3$ (growth-adjuster) and Au decahedra (seeds), and $HAuCl_4$ (precursor). The standard synthesis of NBPs proceeded without disturbance in 90 °C oven for 4 h. In Figure 1A1 and A2, SEM and TEM images clearly show that used seeds are decahedral uniformly and FFT pattern (Figure 1A3) further confirms the penta-twinned structure.[45−47] After the formed Au atoms deposited and grew on decahedra surface, NBPs formed (Figure 1B1). From Figure 1B, these prepared NBPs have uniform shape. Inset in Figure 1B2 is the HRTEM image of selected area marked by the square and the 0.24 nm interplanar spacing is related with {111} of Au. The HRTEM image and corresponding FFT indicate that the NBPs also hold penta-twinned structures (Figure 1B2 and B3).[39] Above observations also show that these NBPs have imperfect bipyramid-shape and their ends are {111}-faceted actually.

On the basis of the results presented in Figure 1, the product evolution from well-defined decahedra to uniform NBPs provides direct and hard evidence for the growth of NBPs that they surely stem from the free-defect overgrowth on decahedral seeds with penta-twinned structure.[39] These used Au decahedral seeds have relatively large size and hence their shape can be identified easily with SEM, TEM, and HAADF technologies (Figure 1A).[45,46] This is convenient for determining how growth happens. Both decahedral seeds and NBPs are penta-twinned, clearly indicating that the preferred growth along ⟨110⟩ on Au seed surface results in the formation of NBP. Ideally, the crystal edges of decahedral seed are lines and their width is equal to atomic diameter. Besides, compared with crystal face, the atomic coordination number on crystal edge is low and this is not favored by energy minimization. For these reasons, the crystal edges become crystal faces with small area. Therefore, each Au decahedral seed actually has 10 {111} facets, 5 small {100} facets. In overgrowth, protecting agents or Ag-based species selectively adsorb on {100} facets with relatively high surface free energy.[39] As a result, the selective deposition on {111} along ⟨110⟩ occurs fast and generates one-dimensional NBP (The detailed growth mechanism will be discussed later).[39] The penta-twinned decahedral Au seeds are determinative to the preferred growth along ⟨110⟩ and the formation of NBPs. Only net-like nanostructures formed without Au decahedral seeds (Supporting Information Figure S1).

Tuning the Au decahedra size allows well controlling the size of NBPs (Figures 2 and S2 (Supporting Information)). For example, when decahedra with 49 nm edge were used as seeds, the resulting NBPs had 220 nm longitudinal length and 60 nm transverse length (Figures 2A and S2A). If decahedra with 37

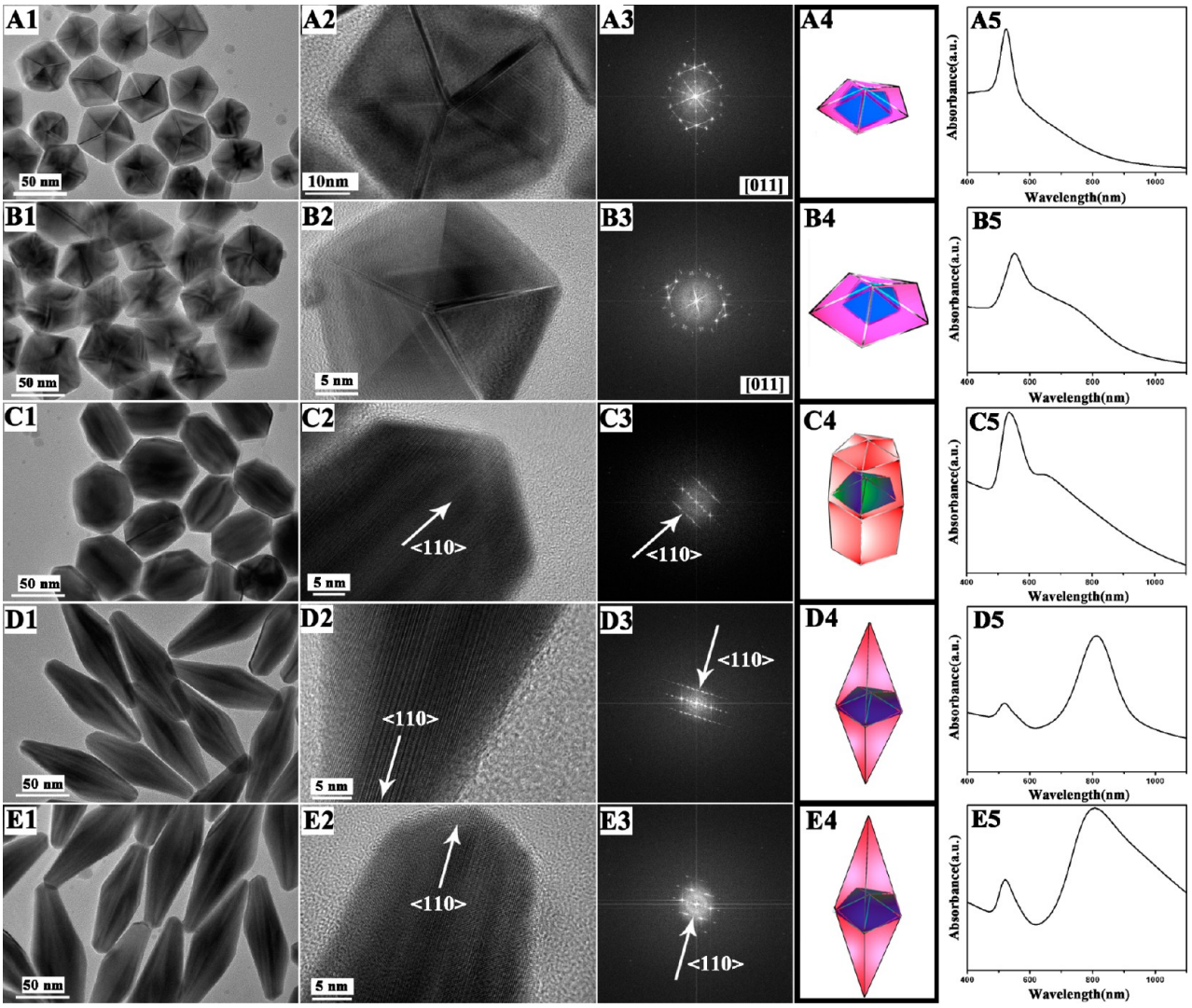

Figure 3. Typical TEM images, HRTEM images, corresponding FFT patterns, and sketches of Au nanostructures prepared by using different MRAAs at 90 °C: (A1−A5) 0; (B1−B5) 1:4; (C1−C5) 1:6; (D1−D5) 1:8; (E1−E5) 1:10. The same decahedral seeds as these shown in Figure 1A1 were used.

nm edge acted as seeds, the longitudinal length and transverse length of corresponding NBPs respectively reduced to 175 and 57 nm (Figures 2B and S2B). Decahedra seeds with 33 nm edge generated NBPs with 157 nm longitudinal length and 47 nm transverse length (Figures 2C and S2C). When Au decahedra with 25 nm edge were added to induce overgrowth, the formed NBPs had 110 nm longitudinal length and 36 nm transverse length (Figures 2D and S2D). The growth time of the NBPs became short with decreasing the size of Au decahedra seeds. For example, decahedral Au seeds with average 49 nm edge needed 210 min to complete the growth of NBPs. However, when decahedra with mean 25 nm edge were used, 60 min reaction could produce NBPs. Prolonging the reaction time (120 min reaction) even caused the distinctive reduction of Ag^{1+} to Ag atoms and consequently Au@Ag NBPs formed (Supporting Information Figure S3). This is in agreement with our previous result that the Ag growth rate on Au decahedra seeds increases with the seeds size decreasing.[46] The size effect demonstrates that the small size seeds have stronger self-catalytic ability.

The surface plasmon resonances mode of noble nanostructures is highly dependent on their shapes.[48−59] For NPs with highly symmetrical structure (nanocube, octahedron, nanoball), only one surface plasmon resonance absorption peak is observed generally.[54] For some one-dimensional Au or Ag nanostructures (nanorod and NBP), they have two surface plasmon resonances responding to the electron oscillations along longitudinal and transverses direction.[55] Among them, the longitudinal surface plasmon resonance is very sensitive to the length change.[56] We used UV−vis spectrophotometer to investigate the surface plasmon resonance of above products. Clearly, bimodal pattern was observed in four cases. Their longitudinal SPR peaks shift from 770 to 970 nm with length increasing (Figure 2A4, B4, C4, and D4). Previously, Guo and co-workers obtained monodispersed Au NBPs using shape-separation technology.[58] Besides, Liu and co-workers measured the light scattering spectrum of single NBP.[39] Compared with their plasmon resonance absorption peak, ours is broad due to the nonuniform size (Supporting Information Figure S2).[39] It has been demonstrated that nanomaterials having absorption in near-infrared region (>800 nm) have promising application in photodynamic therapy.[60] Therefore, these NBPs might have photothermal conversion performance for killing cancer cell.

Scheme 1. (A) Relation between Tetrahedron and Decahedron, (B) Sketches of Length along Transverse and Longitudinal Direction in Different Nanostructures, (C) Sketch of Growth Pattern over MRAA

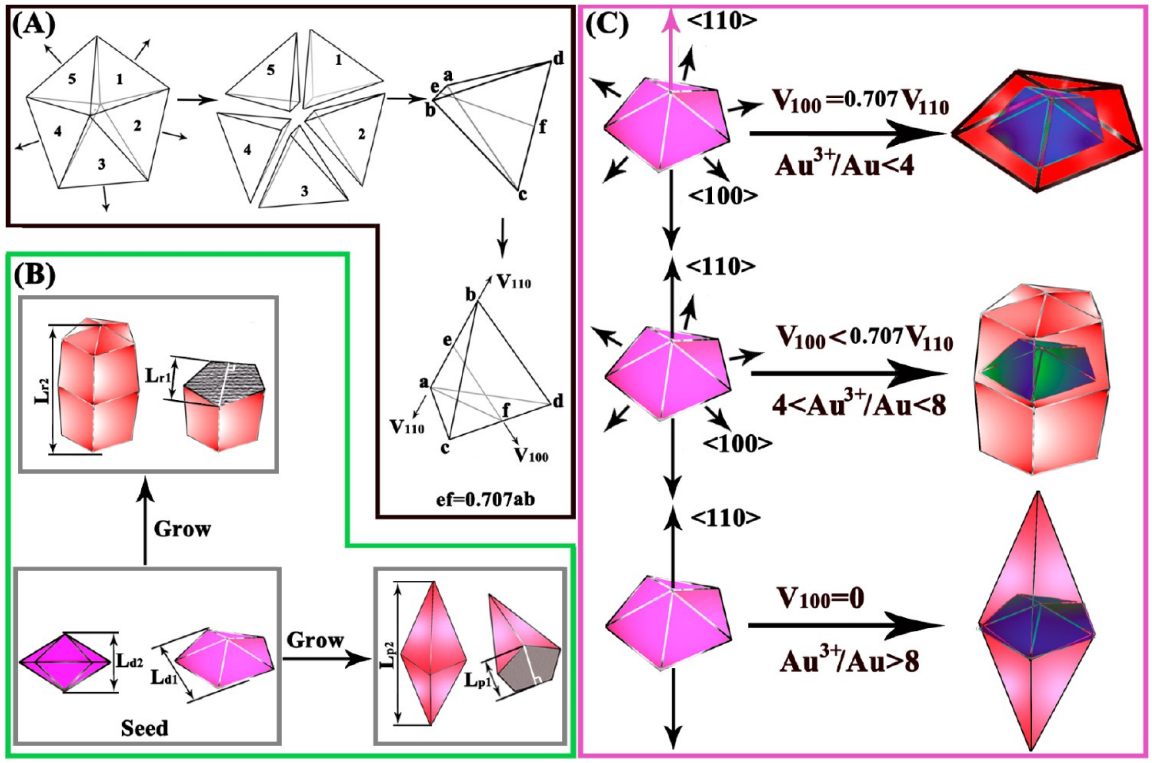

Effect of MRAA. Above result demonstrates that the penta-twinned Au seeds govern the growth and shapes of the resulted products. Besides the structure of seeds, the growth preference also has dependence on the growth rate kinetically which is proportional to MRAA. In all cases discussed above, MRAAs were higher than 9. Therefore, in order to investigate how much the growth rate contributes to the formation of NBPs, we tested different MRAAs (Figure 3). When we increased MRAA, the products shape evolved from decahedron, quasi-nanorod to NBP. Before overgrowth, the seeds are decahedra (Figure 3 A1). The HRTEM image (Figure 3A2) and corresponding FFT pattern (Figure 3A3) confirm the penta-twinned structure. When MRAA is 4, the resulting products still hold decahedral shapes mostly. However, their sizes clearly increased in comparison with seeds. We also carried out the preparation using lower MRAA and similarly only size change was observed (Supporting Information Figure S4B). If MRAA was increased to 6, decahedral products were not observed and most were short quasi-nanorods (Figure 3C). Once MRAA increasing to 8 or 10, only NBPs formed (Figure 3D and E). It is very distinctive that the product shape highly depends on MRAA. The aspect ratio of products increases from 0.67 to 3.2 with MRAA, confirming that high MRAA favors the growth along ⟨110⟩ (Figure S4). For example, when MRAA is 6, the mean aspect ratio of products is 1.4 (Figure S4D). Once MRRA increasing to 8, the aspect ratio of products is 3 (Figure S4E).

Here, we used UV−vis spectra to investigate above shape change with MRAA. For the decahedral seeds with 30 nm edge, their colloids have only one absorption peak and this is consistent with our previous results and other group's reports (Figure 3A5).[44,51,59] After size enhancement (MRAA was 4), the single peak mode was unchanged and the absorption peak had a red shift from 523 to 550 nm, indicating that the sizes of decahedra increased (Figure 3B5). Meanwhile, a weak absorption band (500−700 nm) was also observed, indicating that the growth along ⟨110⟩ also occurred on some seeds (Supporting Information Figure S5). When MRAA was increased to 6, the absorption peak became broad due to the presence shoulder peak, implying that the products have one-dimension feature (Figure 3C5). Meanwhile, the absorption peak related to transverse surface plasmon resonance shifted to longer wavelength and this suggests that transverse length also increased (Figure 3B5). Once MRAA was higher than 8, double-peak absorption mode were distinctively observed (Figure 3D5 and E5), demonstrating that one-dimension NBPs formed. In these cases, the transverse surface plasmon resonance absorption peaks of products have no significant shift compared with that of seeds, which indicates that the transverse length almost was unchanged. It was observed that the longitudinal surface plasmon resonance absorption peaks of products (MRAA is 10) became broad. This is probably due to the fast growth rate which caused an inhomogeneous growth and in turn a broad size distribution. If MRAA was higher than 12, products become highly nonuniform and lots of small sized Au NPs formed owning to additional nucleation, further conforming that high yield synthesis were not favored by too high MRAA (Supporting Information Figure S5).

As is well-known, the shape of nanostructures are due to the comprehensive effect of growth along different directions.[50,61] In our case, the products shapes are primarily determined by the growth along ⟨100⟩ and ⟨110⟩. That is to say, the shape evolution is basically caused by the ratio of growth rate along ⟨100⟩ (V_{100}) and ⟨110⟩ (V_{110}). The ratio of growth rate can be approximately calculated through comparing the length change along ⟨110⟩ and ⟨100⟩ before and after growth. Geometrically, decahedron is composed of 5 tetrahedra (Scheme 1A) and

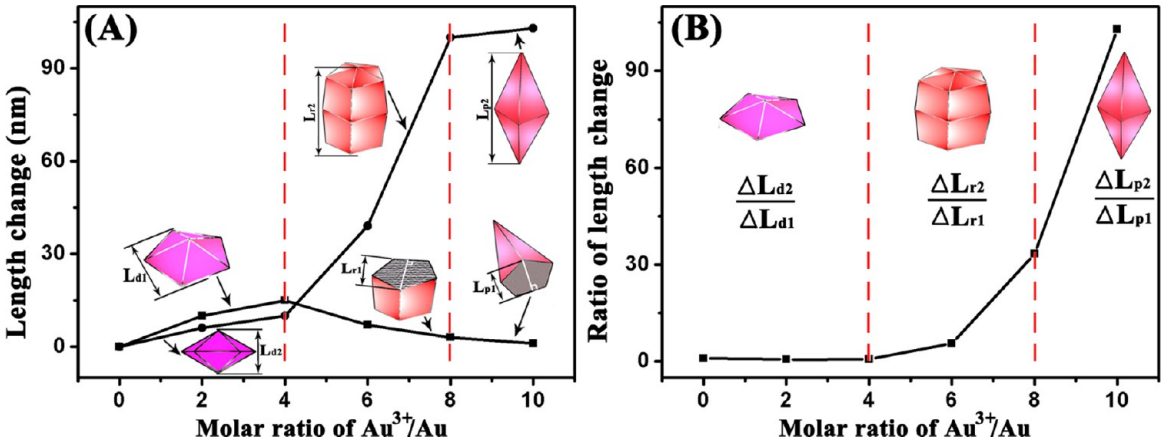

Figure 4. (A) Longitudinal and transverse length changes over MRAA. (B) Ratio of length changes along two directions over MRAA.

therefore we can use the overgrowth on tetrahedron to treat that on decahedron.[45,46] As described in the scheme 1A, *ef* (the length along ⟨100⟩) is 0.707*ab* (*ab* is the length along ⟨110⟩) in tetrahedron or decahedron. In case of penta-twinned nanorod or NBP, *ef* is shorter than 0.707*ab*. Therefore, if products still hold decahedral shape after overgrowth, the increased length of *ef* (Δ*ef*) and that of *ab* (Δ*ab*) also should meet the rule (Δ*ef* = 0.707Δ*ab*). That is to say, V_{100} is equal to $0.707V_{110}$. This case happens when MRAA ranges from 0 to 4 (Figures 3A and B and S4A−C (Supporting Information) and Scheme 1C). Experimentally, if Δ*ef* is smaller than 0.707Δ*ab*, products have other shape rather than decahedron. This is what we see when MRAA is 6 (Figure 3D). When Δ*ef* is close to zero, no observable growth along ⟨100⟩ occurs and only MRAA ranging from 8 to 10 allows this happening. This case can be easily recognized through comparing L_{d1} and L_{p1} or L_{r1} (Scheme 1B). If L_{d1} is close to L_{p1} or L_{r1}, the growth follows this way (Figures 3C−E and S4D−F (Supporting Information) and Scheme 1C).

In order to more clearly show the effect of MRAA, the length changes along ⟨110⟩ and ⟨100⟩ were carefully measured (Figure 4A). It can be seen that Δ*ef* first gradually increased (MRAA is less than 4) and then decreased (MRAA ranges from 4 to 8). When MRAA continues increasing and is higher than 8), Δ*ef* is very small (Δ*ef* = 1 nm) and V_{100} is close to 0 in this case. For Δ*ab*, it increases all the time and its increased rate has dependence on MRAA. When MRAA is lower than 4, the increased rate is small. If MRAA ranges from 4 to 8, the rate increases drastically. With further adding more Au^{3+} precursor (MRAA is higher than 8), the increased rate along ⟨110⟩ becomes small again. It is easily to understand such change of growth rate according to the following equation,

$$M = M_{110} + M_{100} \quad (1)$$

where, *M* is the total amount of introduced Au^{3+}, M_{100} and M_{110} are the amount of consumed Au^{3+} for growth along ⟨100⟩ and ⟨110⟩, respectively. In the case of MRAA less than 4, M_{100} makes up a sizable proportion of *M*. For this reason, the increased rate of longitudinal length with the amount of Au^{3+} is not large. When MRAA ranges from 4 to 8, the proportion of M_{100} significantly reduces with MRAA increasing. However, the proportion of M_{110} further increases. Consequently, the increased rate in longitudinal direction becomes extremely large. Once MRAA is higher than 8, all Au^{3+} ions are consumed for increasing longitudinal length. Nevertheless, the increased rate of longitudinal length became slow. This can be understood easily. Hypothetically, we carry out a seeded growth in which the NBPs shown in Figure 3D are seeds and MRAA is 0.25. Because the NBPs (Figure 3D) have large surface area as active sites and however newly formed Au atoms are relatively few, the length change is not significant. Above observation clearly demonstrates that high MRAA accelerates the growth along ⟨110⟩ and does not favor the growth along ⟨100⟩, facilitating the formation of NBPs or quasi-nanorods.

Interestingly, above observation was inconsistent with that in classical system. For example, Wang's group reported a synthesis of NBPs with improved yield and their MRAA was 325.[56] In our experiment, MRAA higher than 10 caused the failure of preparing NBPs due to significant additional nucleation (Supporting Information Figure S6). Another difference is the effect of MRAA on the growth along ⟨100⟩. In the classic method, although MRAA is much higher, the growth along ⟨100⟩ obviously happens and it is demonstrated by the increased transverse length. For our case, the growth along ⟨100⟩ almost stops completely even MRAA higher than 8. It is difficult to clarify what causes these disagreements because there are many differences between our system and theirs (solvent, stabilizing agent, seed size, et al.). Very possibly, ultrafine seeds used in their system play important roles. Their seeds have small surface area and therefore only {111} facets are unable to provide enough nucleation. Besides, in their system, MRAA is very high and this exacerbates the shortage of nucleation sites on {111}. Under such circumstances, the Au atoms on {100} facets also share responsibility for nucleation sites. Therefore, the growth along ⟨100⟩ also occurs in their system.

Possible Mechanism. Besides growth rate, other two factors are believed to have important impacts on the growth of NBPs, the selective absorption of AgCl which slows down the growth along ⟨100⟩, the competitive absorption of AgCl and newly formed Au atoms on {111}. **(1) The selective absorption of AgCl on {100}.** When $AgNO_3$ was absent, such preferential growth along ⟨110⟩ was not observed (Supporting Information Figure S7). Previously, we reported that the selective absorption of solubilized AgCl species governed the growth of Au nanostructure very possibly.[46] PVP is a common protecting agent which is unable to solubilize AgCl. When PVP acted as protecting agent in a comparison test and other synthetic conditions were unchanged, the preparation of NBPs failed (Supporting Information Figure S8A and B), suggesting that AgCl is key to the growth of NBPs. When

Scheme 2. Sketch of Three Growing Patterns: (A) Decahedra to NBPs; (B) Decahedra to Quasi-Rod Products; (C) Decahedra to Larger Sized Decahedra

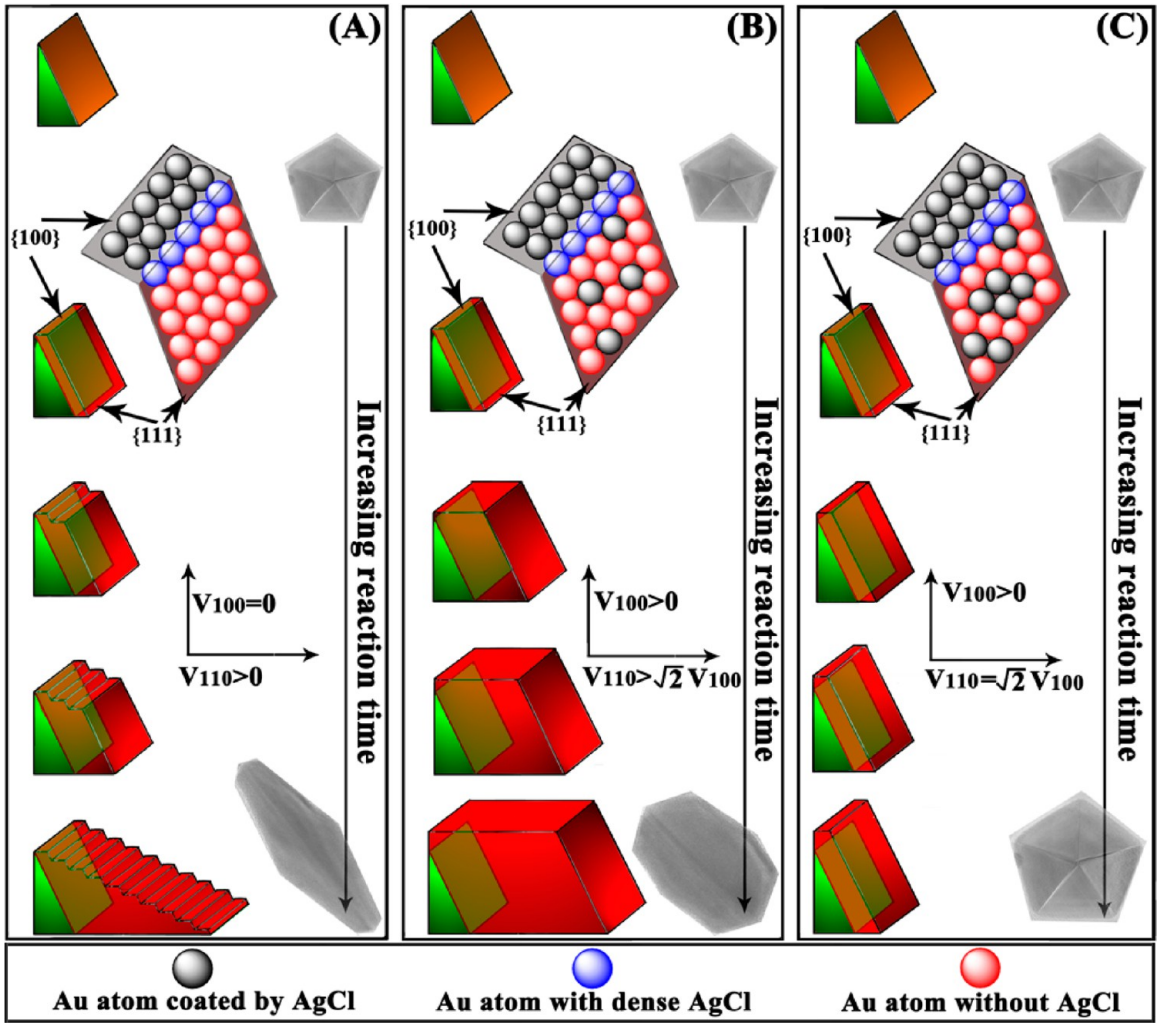

CTAC with weak ability to solubilize AgCl served as surfactant, only a small amount of NBPs formed (Figure S8C and D), further demonstrating that AgCl is key to the selective growth along ⟨110⟩. In general, the growth of any nanostructure involves two stages, nucleation (small sized NPs form and serve as seeds for further growth) and subsequent growth on relatively active sites. For seeded growth, these two stages are completely separated artificially.[62−64] Because of the inhomogeneous surface energy distribution on seeds surface, their crystal shapes have determinant effects on subsequent growth and in turn product shape.[21,39] Besides, the growth environment is also very critical.[65−69] Theoretically, in most cases, seeds are coated by three commonly seen low index facets ({111}, {100}, {110}) and the order energetically (surface free energy) is {110} > {100} > {111}.[29] Therefore, it seems very reasonable that the growth on seeds surface should occur preferentially on {110} or {100}, producing {111}-faceted nanostructures. Practically, the introduction of other substances (polymer, surfactant, inorganic ion) can modulate their surface free energy distribution and hence change the growth perference.[67−69] In the present study, our observations well demonstrate this. As discussed before, although there is no bounding {100} facet on the surface of decahedron in theory, these five crystal edges composing of pentagon actually are {100} facets with small area due to imperfect growth. If there is no AgCl, growth should occur preferentially on these positions because Au atoms here are more active than these on {111}. Introducing $AgNO_3$ leads to forming AgCl species which selectively absorb on {100} due to energy minimization trend. For this reason, the activity of {100} decreases and is lower than that of {111}. Consequently, the selective deposition on {111} happens along ⟨110⟩, producing one-dimension nanostructures. **(2) The competitive absorption between AgCl and newly formed Au atoms on {111}.** To understand how the growth rate affects the products shape, the first important thing is to analyze how surface active site changes with the growth rate of Au atoms. For three kinds of products (NBP, quasi-nanorod, decahedron), their ends are coated by {111} facets. On their side surface, the bounding facets are {100} facets. In growth, the deposition of Au atoms on {100} is not favored due to the selective absorption of AgCl and therefore the growth along ⟨100⟩ is always slower than that along ⟨110⟩.[34,39] The Au atoms on bounding {111} facets have different activity due to the impact of surrounding environment. As illustrated in Scheme 2A, these Au atoms marked by the blue color at edge (AAE) are more active because of low coordination number.[70,71] For this reason, they have the strongest affinity with AgCl and very possibly AgCl absorbs here densely. Although AgCl prefers absorbing on {100}, our

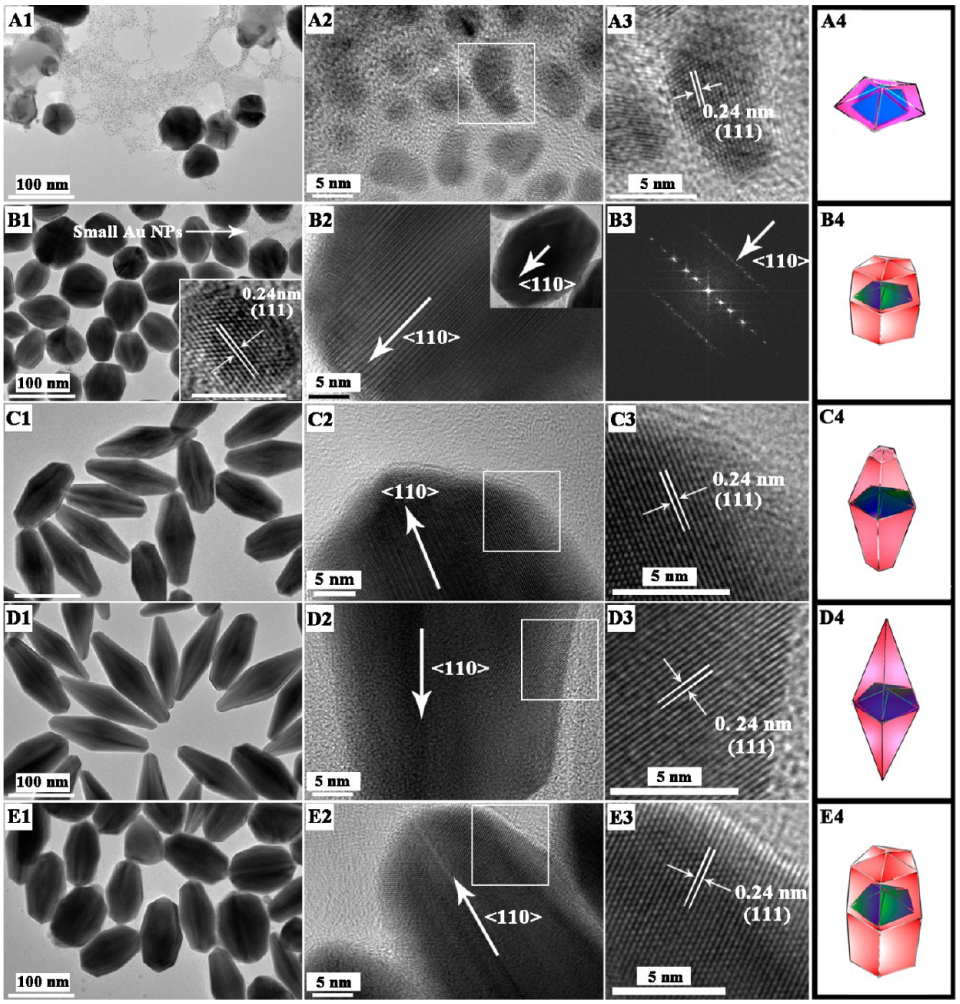

Figure 5. (A1–A4) TEM images, HRTEM images, and sketches of Au nanostructures prepared at 40 °C. (B1–B4) TEM image, HRTEM image, corresponding FFT pattern and sketch of Au nanostructures prepared at 60 °C. (C1–C4) TEM images, HRTEM images, and sketches of Au nanostructures prepared at 80 °C. (D1–D4) TEM images, HRTEM images, and sketches of Au nanostructures prepared at 110 °C. (E1–E4) TEM images, HRTEM images, and sketches of Au nanostructures prepared at 120 °C. The squares (A2, B2, C2, D2, and E2) mark the area of HRTEM image (A3, B3, C3, D3, and E3). The decahedra with 37 nm edge served as seeds, and MRAA was 10.

previous studies show that it also absorbs on {111} and slow down the growth there when excess AgCl species are present.[46] Besides, there is another absorption that the newly formed Au atoms deposit and grow on {111}. Therefore, there is competition between two absorptions which determines how growth occurs and in turn products shape. When MRAA is large, the forming rate of Au atoms is very fast and the concentration of Au atom is high. As a result, the absorption of Au atoms is dominant. In other words, AgCl has no enough time to absorb on {111} and therefore there is very little AgCl here. Under this circumstance, only {100} and the AAE are coated by AgCl densely. Consequently, the deposition of Au atoms on {111} only occurs on these atoms marked by the red ball. However, no Au atom deposits on AAE due to dense absorption of AgCl there. Therefore, AAE and newly deposited Au atoms compose a step. Such growth is repeated until most of Au precursor are consumed, resulting in the formation of NBPs. It is worth noting that there should exist Au atoms with few coating AgCl on {100} sometime and they also can serve as nucleation site for the deposition of Au atoms, because the absorption and desorption of stabilizing agent or other substances on surface are in a dynamic equilibrium.[72,72] Therefore, the growth along ⟨100⟩ cannot be blocked completely and is too slow to observe. If MRAA is low, the concentration of Au atom is relative low and hence AgCl absorb on parts of Au atoms on {111}. This decreases the growth rate along ⟨110⟩ and accelerates the growth along ⟨100⟩ relatively, facilitating the formation of quasi-nanorods (Scheme 2B). Once MRAA further decreases, the absorption of newly formed Au atom lost dominant position. There are more AgCl species absorbing on {111} which heavily reduce the growth rate along ⟨110⟩ and produce decahedra (Scheme 2C). It should be noted that the decreasing nucleation site should also make contribution. The forming rate of Au atoms reduces with time because Au^{3+} precursor is consumed. Theoretically, the growth along ⟨100⟩ should be accelerated. However, experimentally such a result was not observed. Very possibly, the ends of products become sharp and consequently the nucleation sites decreases. For this reason, the concentration of formed Au atom is still relatively high.

Previously, Liu and co-workers studied the growth of NBP.[39] They believed that the growth along the twinning axis did not favor the formation of flat {100} and produced steps. In fact, the growth along twinning axis also prefers flat {100}. For

example, Song's group synthesized Au nanorods through the growth along the twinning axis of Au decahedra.[34] Therefore, the selective absorption of AgCl is responsible for the formation of NBP more possibly. Interestingly, the Au growth on Au decahedra is significantly different in comparison with Ag growth on Au decahedra or Pd nanocubes kinetically. Previously, Xia's group demonstrated that fast growth of Ag yielded Pd@Ag nanocubes and slow growth favored asymmetric growth.[20,74] We found similar results through studying the Ag growth on Au decahedra.[46] However, in the current study, the Au growth does not follow such rule. This difference might be caused by the AgCl. For Ag growth on Pd or Au surface, AgCl has no significant growth-directing effect. However, in case of Au growth, it has essential roles and modulates the growth preference.

Appropriate amount of aqueous ammonia is very important to the growth of NBPs. When aqueous ammonia was less than 10 uL, the growth became slow heavily and no NBPs formed (Supporting Information Figure S10). We also tried to prepare NBPs by introducing more aqueous ammonia to accelerate growth because the reducing ability of DEG becomes strong in alkaline system.[46,65] This strategy is demonstrated to be excellent for preparing Au-tipped Ag nanorods or Au@Ag decahedra.[45,46] However, the preparation of NBPs was successful only when 10 μL aqueous ammonia was added (Supporting Information Figure S9). Aqueous ammonia more than 10 μL produced other shaped products. It is because of this that aqueous ammonia and AgCl can form $Ag(NH_3)^{2+}$ which has no growth-directed effect on Au nanostructures.[75] Hence, 20 uL aqueous ammonia reduces the selectivity of growth and hence the growths along both along ⟨110⟩ and ⟨100⟩ occur, generating quasi-nanorods (Figure S9B). If 30 uL aqueous ammonia was introduced, the growths along both directions were very fast and hence {111}-faceted icosahedra were favored (Figure S9C). Besides, the present plate- and wirelike products show that 30 uL aqueous ammonia resulted in additional nucleation. Once increasing the amount of aqueous ammonia to 50 uL, additional nucleation dominated and most products were net-like (Figure S9D−G). This case is similar to the preparation without Au decahedra seeds (Supporting Information Figure S1), confirming that net-like nanostructures is due to additional nucleation. Unlike the Ag growth on Au decahedron, the Au growth is mainly influenced by the AgCl rather than $Ag(NH_3)^{2+}$. Therefore, the introduction of aqueous ammonia accelerates the reduction of Au^{3+} to Au atom and meanwhile reduces the growth-directed effect of AgCl because of the formation of $Ag(NH_3)^{2+}$. However, for Ag growth, aqueous ammonia only affects the concentration of Ag atom. Thus, the effect of aqueous ammonia on the Au and Ag growth is different. This result also support our conclusion reached in previous report.[46] The effect of Ag-based species on the growth of Au nanostructures is due to the selective absorption of AgCl rather than Ag atoms from under-potential-deposition (UPD). If UPD mechanism works well in our system, the Ag UPD is not determined by the surfactant. Actually the reduction of Ag^+ to Ag atom was observed regardless of which surfactant was used. That is to say, UPD has no strong dependence on surfactant. Hence, the growth of NBPs should be not determined by the type of surfactant. However, as described before, practically only some surfactants (CTAC or PDDA) with ability to solubilize AgCl allows preparing NBPs (Supporting Information Figure S8). This indicates that the solubilized AgCl instead of these deposited Ag on Au surface is a determining factor to the formation of NBPs.

Effect of Reaction Temperature. As well as MRAA, adjusting reaction temperature allows modulating the reaction kinetics through tuning ion, atom, and molecule motion. Therefore, we also performed syntheses at different reaction temperatures and found that it drastically affected the resulting products (Figure 5). When the growth proceeded at 40 °C, the selective growth on seeds surface was inhibited and additional nucleation occurred heavily, generating large amount of small sized Au NPs (Figures 5A and S11 (Supporting Information)). With increasing reaction temperature to 60 °C, additional nucleation was still distinctly observed (Figure 5B and inset). However, additional nucleation greatly reduced compared with the synthesis carried out at 40 °C (Figure 5A). If the reaction was performed at 80 °C, NBPs formed and no additional nucleation was observed (Figure 5C), indicating that the selective growth on seeds surfaces along ⟨110⟩ became fast and dominated. Once further increasing reaction temperature to 90 or 110 °C, the shape of products had no change and however their ends became sharper (Figures 5D and 2C). However, if reaction temperature was increased to 120 °C, products changed from NBPs to quasi-nanorods (Figure 5E). The preparation at 150 °C produced polydispersed products including NBPs, Au@Ag NBPs, and pure Au NPs (Supporting Information Figure S12), suggesting that too high reaction temperature causes significant additional nucleation and reduction from Ag ion to Ag atom.

In our system, high temperature might have two effects, increasing the dissolubility of AgCl and accelerating the reduction from Au ion to Au atom.[46] When the temperature is low, AgCl aggregations coat on seeds surface densely and block the selective growth, favoring additional nucleation and the formation of small sized Au NPs. If temperature becomes higher, AgCl aggregations dissolve and this prefers the selective deposition of Au atoms on seed surface. Besides, increasing reaction temperature also accelerates the reduction of Au ion to Au atoms. As a result, the Au atom concentration becomes higher, facilitating the growth along ⟨110⟩ and the formation of long NBPs. This can be demonstrated by the changes of longitudinal and transverse length (Supporting Information Figure S13). A 60 °C reaction produced products with 60 nm longitudinal length and 73 nm teraservers length (Figure S13A). Compared with seeds, both become long, demonstrating that the growth along ⟨110⟩ and ⟨100⟩ occurs simultaneously. Further elevating temperature (80 and 110 °C) led to a dramatic increase of longitudinal length (Figure S13B and C). However, the transverse length decreased to about 55 and 54 nm which were close to that of seeds, suggesting that no significant growth along ⟨100⟩ happens. This is consistent with the observation that fast growth rate only favors the growth along ⟨110⟩ (Figure 3). A 120 °C reaction temperature, by contrast, reduced the longitudinal length and increased transverse length (Figures 5E and S13D). Meanwhile, the products are close to nanorods. This is understandable thermodynamically. Because high index facets are unstable and not favored by the energy minimization trend, atomic reconstruction often occurs easily. As a result, high index facets change to these with relatively low surface free energy. Besides, high temperature can accelerate atomic reconstruction.[46] Compared with NBPs, quasi-nanorods have relatively stable bounding facets and hence the atomic reconstruction facilitates their formation (Figures 5E and S13D).[46,76] The temperature-

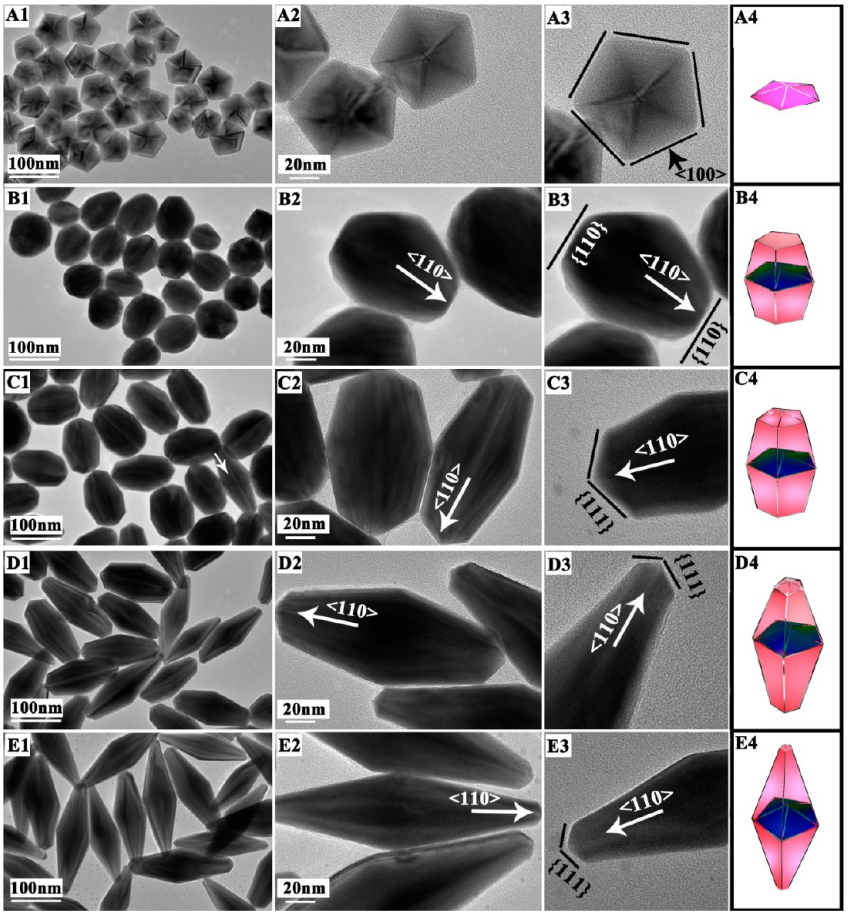

Figure 6. TEM images, high magnification TEM images, HRTEM images, and sketches of Au nanostructures formed in different stages: (A1−A4) 0; (B1−B4) 0.5; (C1−C4) 1.5; (D1−D4) 2.5; (E1−E4) 3.5 h. The decahedra with 49 nm edge acted as seeds, and MRAA was 9.

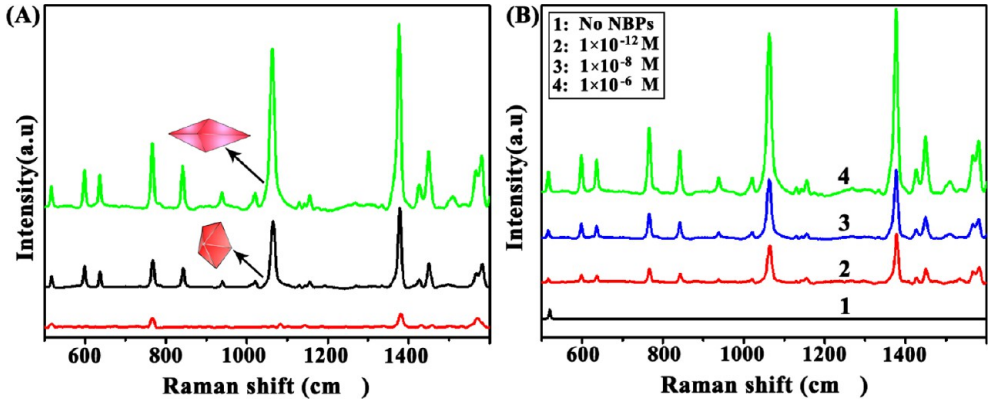

Figure 7. SERS spectra using (A) various shaped Au nanostructures (decahedra shown in Figure 1A and NBPs shown in Figure 1B) as substrate materials (the red curve is recorded using supersaturated suspension of probe molecule in water). (B) NBPs (Figure 1B) as substrate materials with different concentrations of probe molecule.

dependent growth also can be confirmed by the aspect ratio change of products. For example, 60, 80, and 110 °C reaction produced products with 1.1, 2.3, and 3 aspect ratio, respectively (Figure S13), indicating that high temperature prefers the growth along ⟨110⟩. However, the aspect ratio of products prepared at 120 °C reaction reduced to 2.3, demonstrating that atomic reconstruction shortens the longitudinal length.

Effect of Reaction Time. Large sized seeds need relatively long reaction time and allow having enough time to obtain intermediates. In order to investigate the product shape change over reaction time, decahedra with 49 nm edge were chosen as seeds for investigating time-dependent evolution. The products with different reaction times were taken out and observed with TEM and HRTEM. Initially, the seeds have decahedral shape uniformly (Figure 6A). After 30 min, no decahedra were observed and most of products were truncated NBPs (Figure 6B), suggesting that the growth along ⟨110⟩ occurred in this stage. Ninety minutes later, the longitudinal length of truncated NBPs increased (Figure 6C). Some products marked by the arrow in Figure 7C1 already had shapes close to NBP. If

reaction time was prolonged to 150 min, products were NBPs mostly (Figure 6D). When the reaction time was up to 180 min, almost all products were NBPs (Figure 6E). After that, further increasing reaction time was unable to increase longitudinal length of products, implying that the growth of NBPs was completed after 180 min.

It was noted that the end facets of products with different reaction times were not constant. The products with 30 min reaction time have 2 flat ends which indicates that the products in this stage have {110} facets (Figure 6B2). However, the HRTEM images (Figure 6B3, C3, D3, and E3) show that the ends of products with reaction time longer than 30 min are bounded by {111} facets. In comparison with {110}, {111} is favored thermodynamically because its surface free energy is low. The present {110} facets on products with 30 min reaction time might be due to the absorption of AgCl which decreases the atom activity there. In this stage, the products have relatively small surface area and the amount of AgCl is enough to coat the product surface densely. Therefore, {110} facets were observed when reaction time was short. However, with increasing reaction time, the total surface area of products became large and there were no enough AgCl stabilizing {110}. Therefore, {110} facets vanished due to the fast growth rate on products surfaces and {111} facets dominated on the ends. For the NBPs prepared using classical method,[39] their tips are much sharper than ours. Very possibly, high synthetic temperature causes the formation of {111}-faceted tip. Compared with classical synthesis, our reaction temperature is high, which can accelerate the atomic reconstruction and favor the formation of nanostructure with low surface free energy. {111} is the most stable facet, and therefore, {111}-faceted tips form in our system.

SERS. As is well-known, noble metals (Ag and Au) are excellent substrate materials for SERS.[77−89] Their SERS performance has dependence on their shapes and compositions. For example, Han demonstrated that Au NPs with high index facets possessed stronger SERS ability than spherical ones.[78] Another group reported that nanostructures with sharp tips were effective substrate materials.[77,79] Herein, these prepared NBPs have above two features and possibly have good SERS performance. We used 2-naphthalenethiol as probe molecule and investigated the SERS performance of prepared NBPs. For the sake of comparison, we also tested the SERS performance of Au decahedra and recorded the Raman spectrum of 2-naphthalenethiol. Results show that both decahedra and NBPs have SERS performance (Figure 7A). Besides, the SERS performance depends on the shape of substrate materials. Although decahedra have small size and large surface area, their SERS performance is inferior to that of NBPs (Figure 7A). Compared with decahedra, NBPs have two sharp ends and stepped {100} on which lots of high index facets are exposed. Therefore, their strong SERS performance probably stems from these hot spots, sharp tips, edges, and high-energy step atoms. A method reported by other groups was used to calculate the enhancement factor of 2 substrate materials (The details can be seen in the Supporting Information).[87] The enhancement factor of NBPs is 1.3×10^6 and almost four times as high as that of decahedra (3.2×10^5). This result also demonstrates that NBPs are better SERS materials than decahedra. We also investigated the SERS performance of NBPs over the concentrations of probe molecule (Figure 7B). Without NBPs, only one peak (520 cm^{-1}) was observed and it was assigned to Si substrate. After NBPs were treated with different concentrations of probe molecule, the Raman signal of probe molecule was detected. Even at very low concentration of probe molecule (curve 2 in Figure 7B), the signal was still clearly observed, indicating that NBPs could serve as excellent substrate materials. Because the tips of Au NBPs often have stronger affinity with probe molecules than other positions, they possess important application in detection of single molecule via SERS.[87]

4. CONCLUSION

We have demonstrated that the overgrowth on Au decahedral seeds (edge size ranging from 25 to 49 nm) allows preparing NBPs with uniform shape and controlled size (longitudinal length from 110 to 210 nm; transverse length from 36 to 70 nm). For these used decahedral seeds have well-defined shape and large size, the growth of NBPs can be observed with TEM easily. The successful preparation of NBPs provides hard evidence for the growth of NBPs that they surely stem from the overgrowth on penta-twinned decahedra. Besides, the present study shows that the stepped growth of NBP is related with the growth kinetics of Au and favored by fast growth. Slow growth only facilitates size enhancement of decahedral seeds or the formation of Au quasi-nanorods. The effect of growth rate possibly is due to the competitive adsorption between AgCl and newly formed Au atoms on {111}. These two absorptions on {111} are governed by the forming rate of Au atom. Fast rate facilitates the absorption of newly formed Au atoms and stepped growth is favored, producing NBPs. Otherwise, AgCl species considerably absorb on {111} and decahedra or quasi-nanorods are generated. These prepared NBPs exhibit excellent SERS performance due to present many stepped atoms and tips on their surfaces.

■ ASSOCIATED CONTENT

Ⓢ Supporting Information

Other TEM, EDS, and HRTEM results are included. This material is available free of charge via the Internet at http://pubs.acs.org.

■ AUTHOR INFORMATION

Corresponding Authors

*E-mail: bachier@163.com (Y.Y.).
*E-mail: smhuang@wzu.edu.cn (S.H.).

Notes

The authors declare no competing financial interest.

■ ACKNOWLEDGMENTS

This work was supported by the NSFC (21101120, 21173159, 51025207), Zhejiang science and technology project (2010C31039), and Lucheng science and technology project (T100106).

■ REFERENCES

(1) Sun, Y. G.; Xia, Y. N. *Science* **2002**, *298*, 2176−2179.
(2) Gontard, L. C.; Dunin-Borkowski, R. E.; Ozkaya, D. *J. Microsc.* **2008**, *232*, 248−259.
(3) Xiao, J.; Qi, L. *Nanoscale* **2011**, *3*, 1383−1396.
(4) Zhang, Q.; Ge, J.; Goebl, J.; Hu, Y.; Sun, Y.; Yin, Y. *Adv. Mater.* **2010**, *22*, 1905−1909.
(5) Huang, X.; Neretina, S.; El-Sayed, M. A. *Adv. Mater.* **2009**, *21*, 4880−4910.
(6) DeSantis, C. J.; Weiner, R. J.; Radmilovic, A.; Bower, M. M.; Skrabalak, S. E. *J. Phys. Chem. Lett.* **2013**, *4*, 3072−3082.

(7) Porter, N. S.; Wu, H.; Quan, Z.; Fang, J. *Acc. Chem. Res.* **2013**, *46*, 1867−1877.
(8) Huang, X.; Zheng, N. *J. Am. Chem. Soc.* **2009**, *131*, 4602−4603.
(9) Li, J.; Han, J.; Xu, T.; Guo, C.; Bu, X.; Zhang, H.; Wang, L.; Sun, H.; Yang, B. *Langmuir* **2013**, *29*, 7102−7110.
(10) Tsung, C. K.; Kou, X.; Shi, Q.; Zhang, J.; Yeung, M. H.; Wang, J.; Stucky, G. D. *J. Am. Chem. Soc.* **2006**, *128*, 5352−5353.
(11) Ruan, L.; Chiu, C.-Y.; Li, Y.; Huang, Y. *Nano Lett.* **2011**, *11*, 3040−3046.
(12) Gomez-Graña, S.; Goris, B.; Altantzis, T.; Fernández-López, C.; Carbó-Argibay, E.; Guerrero-Martínez, A.; Almora-Barrios, N.; López, N.; Pastoriza-Santos, I.; Pérez-Juste, J.; Bals, S.; Van Tendeloo, G.; Liz-Marzán, L. M. *J. Phys. Chem. Lett.* **2013**, *4*, 2209−2216.
(13) Wang, A.; Peng, Q.; Li, Y. *Chem. Mater.* **2011**, *23*, 3217−3222.
(14) Langille, M. R.; Personick, M. L.; Zhang, J.; Mirkin, C. A. *J. Am. Chem. Soc.* **2012**, *134*, 14542−14554.
(15) Orendorff, C. J.; Gearheart, L.; Janaz, N. R.; Murphy, C. *Phys. Chem. Chem. Phys.* **2006**, *8*, 165−170.
(16) Sun, X.; Guo, S.; Liu, Y.; Sun, S. *Nano Lett.* **2012**, *12*, 4859−4863.
(17) Zhang, Q.; Xie, J.; Liang, J.; Lee, J. Y. *Adv. Funct. Mater.* **2009**, *19*, 1387−1398.
(18) Peng, Z.; Wu, J.; Yang, H. *Chem. Mater.* **2009**, *22*, 1098−1106.
(19) Wang, C.; Tian, W.; Ding, Y.; Ma, Y.; Wang, Z. L.; Markovic, N. M.; Stamenkovic, V. R.; Daimon, H.; Sun, S. J. *Am. Chem. Soc.* **2010**, *132*, 6524−6529.
(20) Zhu, C.; Zeng, J.; Tao, J.; Johnson, M. C.; Schmidt-Krey, I.; Blubaugh, L.; Zhu, Y.; Gu, Z.; Xia, Y. *J. Am. Chem. Soc.* **2012**, *134*, 15822−15831.
(21) DeSantis, C. J.; Skrabalak, S. E. *J. Am. Chem. Soc.* **2012**, *135*, 10−13.
(22) Lu, C. L.; Prasad, K. S.; Wu, H. L.; Ho, J. A. A.; Huang, M. H. *J. Am. Chem. Soc.* **2010**, *132*, 14546−14553.
(23) Guo, S.; Wang, E. *Nano Today* **2011**, *6*, 240−264.
(24) Khi, N. T.; Yoon, J.; Kim, H.; Lee, S.; Kim, B.; Baik, H.; Kwon, S. J.; Lee, K. *Nanoscale* **2013**, *5*, 5738−5742.
(25) Niu, W.; Xu, G. *Nano Today* **2011**, *6*, 265−285.
(26) Alkilany, A. M.; Nagaria, P. K.; Hexel, C. R.; Shaw, T. J.; Murphy, C. J.; Wyatt, M. D. *Small* **2009**, *5*, 701−708.
(27) Hong, J.; Kang, S. W.; Choi, B.; Kim, D.; Lee, S. B.; Han, S. W. *ACS Nano* **2012**, *6*, 2410−2419.
(28) Ye, X.; Gao, Y.; Chen, J.; Reifsnyder, D. C.; Zheng, C.; Murray, C. B. *Nano Lett.* **2013**, *13*, 2163−2171.
(29) Yin, Y.; Erdonmez, C.; Aloni, S.; Alivisatos, P. *J. Am. Chem. Soc.* **2006**, *128*, 12671−12673.
(30) Wang, Z. L. *J. Phys. Chem. B* **2000**, *104*, 1153−1175.
(31) Ma, Y.; Li, W.; Cho, E. C.; Li, Z.; Yu, T.; Zeng, J.; Xie, Z.; Xia, Y. *ACS Nano* **2010**, *4*, 6725−6734.
(32) Fan, F.; Liu, D.; Wu, Y.; Duan, S.; Xie, Z.; Jiang, Z.; Tian, Z. Q. *J. Am. Chem. Soc.* **2008**, *130*, 6949−6950.
(33) Wang, F.; Sun, L.-D.; Feng, W.; Chen, H. J.; Yeung, M. H.; Wang, J. F.; Yan, C.-H. *Small* **2010**, *6*, 2566−2575.
(34) Seo, D.; Yoo, C. I.; Jung, J.; Song, H. *J. Am. Chem. Soc.* **2008**, *130*, 2940−2941.
(35) Tsuji, M.; Miyamae, N.; Lim, S.; Kimura, K.; Zhang, X.; Hikino, S.; Nishio, M. *Cryst. Growth Des.* **2006**, *6*, 1801−1807.
(36) Tsuji, M.; Ikedo, K.; Matsunaga, M.; Uto, K. *CrystEngComm* **2012**, *14*, 3411−3423.
(37) Burgin, J.; Liu, M.; Guyot-Sionnest, P. *J. Phys. Chem. C* **2008**, *112*, 19279−19282.
(38) Lombardi, A.; Loumaigne, M.; Crut, A.; Maioli, P.; Del Fatti, N.; Vallée, F.; Spuch-Calvar, M.; Burgin, J.; Majimel, J.; Tréguer-Delapierre, M. *Langmuir* **2012**, *28*, 9027−9033.
(39) Liu, M.; Guyot-Sionnest, P. *J. Phys. Chem. B* **2005**, *109*, 22192−22200.
(40) Nome, R. A.; Guffey, M. J.; Scherer, N. F.; Gray, S. K. *J. Phys. Chem. A* **2009**, *113*, 4408−4415.
(41) Burgin, J.; Florea, I.; Majimel, J.; Dobri, A.; Ersen, O.; Tréguer-Delapierre, M. *Nanoscale* **2012**, *4*, 1299−1303.
(42) Zhang, W.; Johnny Goh, H. Y.; Firdoz, S.; Lu, X. *Chem.—Eur. J.* **2013**, *16*, 12732−12738.
(43) Elechiguerra, J. L.; Reyes-Gasga, J.; Yacaman, M. J. *J. Mater. Chem.* **2006**, *16*, 3906−3919.
(44) Novo, C.; Funston, A. M.; Mulvaney, P. *Nat. Nanotechnol.* **2008**, *3*, 598−602.
(45) Yang, Y.; Wang, W.; Li, X.; Chen, W.; Fan, N.; Zou, C.; Chen, X.; Xu, X.; Zhang, L.; Huang, S. *Chem. Mater.* **2013**, *25*, 34−41.
(46) Li, X.; Yang, Y.; Zhou, G.; Han, S.; Wang, W.; Zhang, L.; Chen, W.; Zou, C.; Huang, S. *Nanoscale* **2013**, *5*, 4976−4985.
(47) Seo, D.; Yoo, C. I.; Im Sik, C.; Park, S. M.; Ryu, S.; Song, H. *J. Phys. Chem. C* **2008**, *112*, 2469−2475.
(48) Sánchez-Iglesias, A.; Pastoriza-Santos, I.; Pérez-Juste, J.; Rodríguez-González, B.; García de Abajo, F. J.; Liz-Marzán, L. M. *Adv. Mater.* **2006**, *18*, 2529−2534.
(49) Talapin, D. V.; Lee, J.; Kovalenko, M. V.; Shevchenko, E. V. *Chem. Rev.* **2010**, *110*, 389−458.
(50) Tao, A.; Habas, S.; Yang, P. *Small* **2008**, *4*, 310−325.
(51) Rycenga, M.; Cobley, C. M.; Zeng, J.; Li, W. Y.; Moran, C. H.; Zhang, Q.; Qin, D.; Xia, Y. N. *Chem. Rev.* **2011**, *111*, 3669−3712.
(52) Sau, T. K.; Rogach, A. L. *Adv. Mater.* **2010**, *22*, 1781−1825.
(53) Rodríguez-Fernández, J.; Novo, C.; Myroshnychenko, V.; Funston, A. M.; Sánchez-Iglesias, A.; Pastoriza-Santos, I.; Pérez-Juste, J.; García de Abajo, F. J.; Liz-Marzán, L. M.; Mulvaney, P. *J. Phys. Chem. C* **2009**, *113*, 18623−18631.
(54) Chen, H. J.; Kou, X. S.; Yang, Z.; Ni, W. H.; Wang, J. F. *Langmuir* **2008**, *24*, 5233−5237.
(55) Lee, S.; Mayer, K. M.; Hafner, J. H. *Anal. Chem.* **2009**, *81*, 4450−4455.
(56) Kou, X. S.; Ni, W. H.; Tsung, C.-K.; Chan, K.; Lin, H.-Q.; Stucky, G. D.; Wang, J. F. *Small* **2007**, *3*, 2103−2113.
(57) Li, B.; Long, R.; Zhong, X.; Bai, Y.; Zhu, Z.; Zhang, X.; Zhi, M.; He, J.; Wang, C.; Li, Z.-Y.; Xiong, Y. *Small* **2012**, *8*, 1710−1716.
(58) Guo, Z.; Wan, Y.; Wang, M.; Xu, L.; Lu, X.; Yang, G.; Fang, K.; Gu, N. *Colloids Surf. A* **2012**, *414*, 492−497.
(59) Perez-Juste, J.; Pastoriza-Santos, I.; Liz-Marzán, L. M.; Mulvaney, P. *Coord. Chem. Rev.* **2005**, *249*, 1870−1901.
(60) Cheng, L.-C.; Huang, J.-H.; Chen, H. M.; Lai, T.-C.; Yang, K.-Y.; Liu, R.-S.; Hsiao, M.; Chen, C. H.; Her, L.-J.; Tsai, D. P. *J. Mater. Chem.* **2012**, *22*, 2244.
(61) Sun, J.; Guan, M.; Shang, T.; Gao, C.; Xu, Z.; Zhu, J. *Cryst. Growth Des.* **2008**, *8*, 906−910.
(62) Xia, X.; Xia, Y. *Nano Lett.* **2012**, *12*, 6038−6042.
(63) Gong, J.; Zhou, F.; Li, Z.; Tang, Z. *Langmuir* **2012**, *28*, 8959−8964.
(64) Dai, Y.; Mu, X. L.; Tan, Y. M.; Lin, K. Q.; Yang, Z. L.; Zheng, N. F.; Fu, G. *J. Am. Chem. Soc.* **2012**, *134*, 7073−7080.
(65) Li, C.; Shuford, K.; Chen, M.; Lee, E.; Cho, S. O. *ACS Nano* **2008**, *2*, 1760−1769.
(66) Song, H.; Kim, F.; Connor, S.; Somorjai, G. A.; Yang, P. D. *J. Phys. Chem. B* **2005**, *109*, 188−193.
(67) Gao, J.; Bender, C. M.; Murphy, C. J. *Langmuir* **2003**, *19*, 9065−9070.
(68) Chen, M.; Wu, B.; Yang, J.; Zheng, N. *Adv. Mater.* **2012**, *24*, 862−879.
(69) Millstone, J. E.; Wei, W.; Jones, M. R.; Yoo, H. J.; Mirkin, C. A. *Nano Lett.* **2008**, *8*, 2526−2529.
(70) Zhou, Z.-Y.; Tian, N.; Li, J.-T.; Broadwell, I.; Sun, S.-G. *Chem. Soc. Rev.* **2011**, *40*, 4167−4185.
(71) Wang, F.; Li, C.; Sun, L.-D.; Wu, H.; Ming, T.; Wang, J.; Yu, J. C.; Yan, C.-H. *J. Am. Chem. Soc.* **2010**, *133*, 1106−1111.
(72) Goddard, P. J.; Schwaha, K.; Lambert, R. M. *Surf. Sci.* **1978**, *71*, 351−363.
(73) Schlenoff, J. B.; Li, M.; Ly, H. *J. Am. Chem. Soc.* **1995**, *117*, 12528−12536.
(74) Zeng, J.; Zhu, C.; Tao, J.; Jin, M.; Zhang, H.; Li, Z.; Zhu, Y.; Xia, Y. *Angew. Chem., Int. Ed.* **2012**, *51*, 2354−2358.
(75) Lyu, L.-M.; Huang, M. H. *J. Phys. Chem. C* **2011**, *115*, 17768−17773.

(76) Wang, Z. L.; Gao, R. P.; Nikoobakht, B.; El-Sayed, M. A. *J. Phys. Chem. B* **2000**, *104*, 5417−5420.
(77) Zhang, L.-F.; Zhong, S.-L.; Xu, A.-W. *Angew. Chem., Int. Ed.* **2013**, *52*, 645−649.
(78) Hong, J. W.; Lee, S.-U.; Lee, Y. W.; Han, S. W. *J. Am. Chem. Soc.* **2012**, *134*, 4565−4568.
(79) Tang, X. L.; Jiang, P.; Ge, G. L.; Tsuji, M.; Xie, S. S.; Guo, Y. J. *Langmuir* **2008**, *24*, 1763−1768.
(80) Vigderman, L.; Zubarev, E. R. *Langmuir* **2012**, *28*, 9034−9040.
(81) Garcia-Leis, A.; Garcia-Ramos, J. V.; Sanchez-Cortes, S. *J. Phys. Chem. C* **2013**, *117*, 7791−7795.
(82) Tian, Z.-Q.; Ren, Q.; Wu, D.-Y. *J. Phys. Chem. B* **2002**, *106*, 9463−9483.
(83) Xiong, Y. J.; McLellan, J. M.; Chen, J. Y.; Yin, Y. D.; Li, Z. Y.; Xia, Y. N. *J. Am. Chem. Soc.* **2005**, *127*, 17118−17127.
(84) Yang, M. X.; Chen, T.; Lau, W. S.; Wang, Y.; Tang, Q. H.; Yang, Y. H.; Chen, H. *Small* **2009**, *5*, 198−202.
(85) Pazos-Perez, N.; Garcia de Abajo, F. J.; Fery, A.; Alvarez-Puebla, R. A. *Langmuir* **2012**, *28*, 8909−8914.
(86) Wei, W.; Li, S.; Millstone, J. E.; Banholzer, M. J.; Chen, X.; Xu, X.; Schatz, G. C.; Mirkin, C. A. *Angew. Chem., Int. Ed.* **2009**, *48*, 4210−4212.
(87) Le Ru, E. C.; Grand, J.; Sow, I.; Somerville, W. R. C.; Etchegoin, P. G.; Treguer-Delapierre, M.; Charron, G.; Félidj, N.; Lévi, G.; Aubard, J. *Nano Lett.* **2011**, *11*, 5013−5019.
(88) Hwang, H.; Kim, S.-H.; Yang, S.-M. *Lab Chip* **2011**, *11*, 87−92.
(89) Tang, H.; Meng, G.; Huang, Q.; Zhang, Z.; Huang, Z.; Zhu, C. *Adv. Funct. Mater.* **2012**, *22*, 218−224.